



Article

A Novel Mechanism Based on Oxygen Vacancies to Describe Isobutylene and Ammonia Sensing of p-Type Cr₂O₃ and Ti-Doped Cr₂O₃ Thin Films

Pengfei Zhou ^{1,2,3,†}, Jone-Him Tsang ^{2,†}, Chris Blackman ^{2,*}, Yanbai Shen ³, Jinsheng Liang ¹, James A. Covington ⁴, John Saffell ⁵ and Ehsan Danesh ⁶

- 1 Key Laboratory of Special Functional Materials for Ecological Environment and Information, Hebei University of Technology, Ministry of Education, Tianjin 300130, China; zhoupengfei@hebut.edu.cn (P.Z.); liangjinsheng@hebut.edu.cn (J.L.)
- Department of Chemistry, University College London, London WC1H 0AJ, UK; jone-him.tsang.16@alumni.ucl.ac.uk
- School of Resources and Civil Engineering, Northeastern University, Shenyang 110819, China; shenyanbai@mail.neu.edu.cn
- School of Engineering, University of Warwick, Coventry CV4 7AL, UK; j.a.covington@warwick.ac.uk
- NosmoTech Ltd., Cambridge CB3 0AZ, UK; john@nosmotech.com
- ⁶ Advanced Sensing Technologies Ltd., London N12 8FA, UK; e.danesh@ieee.org
- * Correspondence: c.blackman@ucl.ac.uk
- [†] These authors contributed equally to this work.

Abstract: Gas sensors based on metal oxide semiconductors (MOS) have been widely used for the detection and monitoring of flammable and toxic gases. In this paper, p-type Cr_2O_3 and Tidoped Cr_2O_3 (CTO) thin films were synthesized using an aerosol-assisted chemical vapor deposition (AACVD) method. Detailed analysis of the thin films deposited, including structural information, their elemental composition, oxidation state, and morphology, was investigated using XRD, Raman analysis, SEM, and XPS. All the gas sensors based on pristine Cr_2O_3 and CTO exhibited a reversible response and good sensitivity to isobutylene (C_4H_8) and ammonia (NH $_3$) gases. Doping Ti into the Cr_2O_3 lattice improves the response of the CTO-based sensors to C_4H_8 and NH $_3$. We describe a novel mechanism for the gas sensitivity of p-type metal oxides based on variations in the oxygen vacancy concentration.

Keywords: Cr₂O₃; Ti-doped; AACVD; thin films; gas sensor; mechanism



Citation: Zhou, P.; Tsang, J.-H.; Blackman, C.; Shen, Y.; Liang, J.; Covington, J.A.; Saffell, J.; Danesh, E. A Novel Mechanism Based on Oxygen Vacancies to Describe Isobutylene and Ammonia Sensing of p-Type Cr₂O₃ and Ti-Doped Cr₂O₃ Thin Films. *Chemosensors* **2024**, *12*, 218. https://doi.org/10.3390/ chemosensors12100218

Received: 11 September 2024 Revised: 15 October 2024 Accepted: 16 October 2024 Published: 18 October 2024



Copyright: © 2024 by the authors. Licensee MDPI, Basel, Switzerland. This article is an open access article distributed under the terms and conditions of the Creative Commons Attribution (CC BY) license (https://creativecommons.org/licenses/by/4.0/).

1. Introduction

Volatile organic compounds (VOCs), including ammonia and hydrocarbons, are ubiquitous, and their detection has been employed for the monitoring of food and beverages, agricultural produce, pharmaceuticals, and health [1]. Certain VOCs are highly toxic and/or carcinogenic and may cause both short- and long-term health issues (e.g., allergies or cancer) as well as impact our ecosystem [2]. Even though the human nose serves as a highly sensitive sensing system, it still fails when low-concentration or odorless toxic gases—which pose a serious threat to human health—need to be detected [3,4], so the development of a low-cost, simple-to-operate VOC sensor is of great current interest.

Gas sensors based on metal oxide semiconductors (MOSs) are commercially available and have been widely used in the detection and monitoring of flammable and toxic gases [5]. MOS-based sensors are cheap, reliable, consume relatively low power, and have good sensitivity, due to a wide conductivity range and a robust structure, making them an ideal gas-sensing material [6]. Compared to the commercially successful n-type SnO_2 and WO_3 sensors, p-type MOS-based sensors, such as Cr_2O_3 , CuO, and NiO, have received relatively little attention [7]. As a typical p-type semiconductor, Cr_2O_3 has been used in

gas sensing [8], catalysis [9], and electrochemical devices [10]. It is reported that doping titanium into Cr₂O₃ is an effective method to enhance the gas-sensing performance of pristine Cr₂O₃ [11]. Ti-doped Cr₂O₃ (CTO) MOSs are also good p-type materials for use in gas sensors, due to their tolerance towards humidity, good baseline stability, and reasonable sensitivity. CTO-based sensors are especially good for the detection of trace quantities of reducing gases in air (such as H_2S , CO, or ethanol vapor), with operating temperatures ranging from 300 to 500 °C [12,13]. Shaw [14] reported the deposition of Cr_{2-x}Ti_xO₃ thin films on sensor substrates using a variety of techniques—including screen printing, atmospheric pressure chemical vapor deposition (APCVD), and flame fusion methodsand investigated their gas response to CO and ethanol. Du [15] used electrostatic sprayassisted vapor deposition (ESAVD) at 650 °C to prepare Cr_{2-x}Ti_xO₃ films for the detection of NH₃. The results showed that the sensitivity of Cr_{1.8}Ti_{0.2}O₃ films to 500 ppm NH₃ at 500 °C was around 1.45. To further investigate the effect of different Ti-doping levels on $Cr_{2-x}Ti_xO_3$, Du [16] carried out the synthesis and characterization of $Cr_{2-x}Ti_xO_3$ with different nominal compositions using the ESAVD technique. Of all the CTO sensorsprepared with varying compositions—Cr_{1.7}Ti_{0.3}O₃ exhibited the highest gas sensitivity. This sensor exhibited a gas response of 2.90 when exposed to 500 ppm NH $_3$ at 200 $^{\circ}\text{C}$ and also revealed good sensitivity to ethanol vapor at 400 °C. Conde-Gallardo [17] found that the conductivity of $Cr_{2-x}Ti_xO_3$ films deposited by aerosol-assisted CVD (AACVD), using copper acetylacetonate and titanium butoxide precursors dissolved in isopropanol, was dependent on the degree of Ti-substitution (conductivity decreased with increasing Ti), although they did not measure the gas-sensing properties.

AACVD has been widely implemented to prepare homogenous and uniform thin films and can effectively generate high-purity MOSs [18]. It has a key advantage over alternative methods of sensor material synthesis in that it combines both material synthesis and device integration in a single step. The AACVD process has attracted attention over other CVD processes due to its characteristics of easy operation, low cost, higher deposition rates, and flexibility in tuning thin-film micro/nanostructures [19].

This work focused on the synthesis of Cr₂O₃ and Ti-doped Cr₂O₃ thin films via the AACVD method and demonstrated the relative sensitivity of the materials to the gases ammonia (NH₃) and C_4H_8 . NH₃ is a colorless gas with corrosive properties and a strong pungent odor. Severe damage is caused to the throat, lungs, eyes, and skin, even at low NH₃ concentrations [20]. Moreover, it is reported that exposure to an NH₃ atmosphere exceeding 50 ppm for a long time leads to serious pathological changes in organs such as the liver and kidneys [21] and also results in serious health issues, including respiratory distress, eye irritation, and skin problems [22]. NH₃ is also a metabolite in breath exhaled from the human body, which can be used as a marker of end-stage renal disease (ESRD) for a nondestructive diagnosis in clinical medicine (average 4.88 ppm; range 0.82–14.7 ppm) [23]. As far as we know, this report is also the first time that CTO sensors have been used to detect C₄H₈, a model alkene VOC. The chemical composition and morphological structure of the Cr₂O₃ and CTO thin films were characterized using XRD, Raman analysis, SEM, and XPS. To understand how the conductivity of CTO may change upon exposure to these gases, we present the first description of a gas-sensing mechanism for p-type MOSs, based on varying concentrations of oxygen vacancies in the sensing material.

2. Experimental Section

2.1. Synthesis of Cr₂O₃ and CTO Thin Films

The deposition of Cr_2O_3 and CTO thin films was achieved via the AACVD technique in a homemade reactor equipped with a water-cooling system in the proximity of the inlet to minimize the pre-reaction of precursors. A schematic of the AACVD technique is shown in Figure 1.

To prepare the Cr₂O₃ films, alumina gas-sensor platforms (with interdigitated screenprinted gold electrodes) were first cleaned with acetone and deionized water before use and were then set onto a base and covered with a mask. These were then placed into the

reactor and heated to 340 °C. A solution of chromium hexacarbonyl (0.1 g, 0.454 mmol) in methanol (40.0 mL) was prepared and aerosols of the solution were formed using an ultrasonic humidifier operated at 2 MHz, with the aerosols then transported to the reactor by a N_2 gas carrier at a flow rate of 1000 standard cubic centimeters per minute (sccm). After ~10 cm³ of the precursor solution had been transported, the substrate and mask were rotated 90° and the deposition process continued; this was repeated four times to ensure homogeneous coverage of the thin films across the sensors. Once the precursor solution was exhausted, the heating temperature and flow rate were reduced to 100 °C and 300 sccm, respectively. After deposition, the dark green thin films obtained were annealed for 24 h at variable temperatures and, respectively, named as Cr_2O_3 -1, Cr_2O_3 -2, and Cr_2O_3 -3, corresponding to the annealing temperatures of 500, 600, and 700 °C.

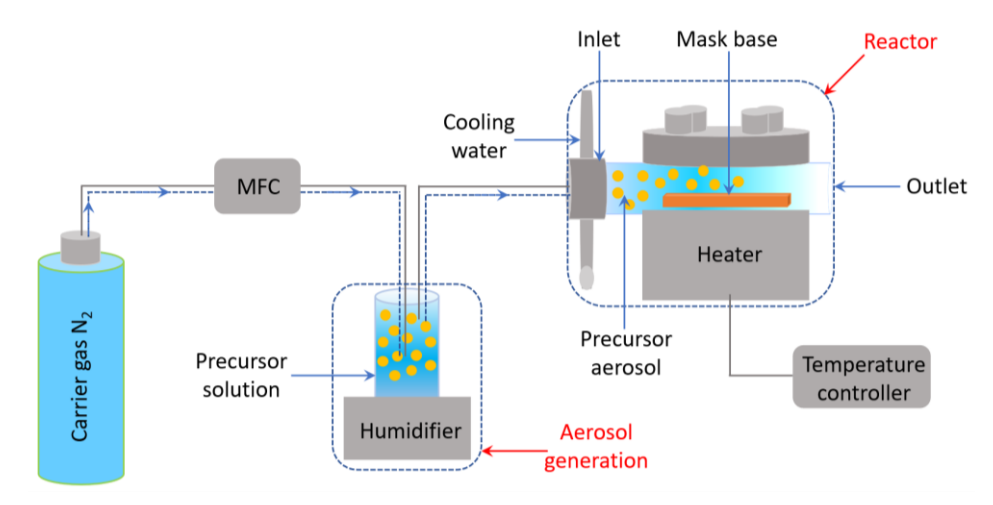


Figure 1. Schematic diagram of an aerosol-assisted CVD.

For the synthesis of CTO thin films, a solution of 0.22 g (0.775 mmol) titanium diisopropoxide bis-(acetylacetonate) (TDBAA) and 15.0 mL methanol was prepared, then 3.0 cm 3 of this TDBAA–methanol solution was added to the chromium solution (as previously prepared) and stirred to obtain a precursor solution with a Cr:Ti molar ratio of Cr_{1.5}Ti_{0.5}. Aerosols of this solution were again generated via a humidifier and transported by a N₂ gas carrier, but this time at a flow rate of 1500 sccm (to provide more homogeneous Ti-incorporation). For the CTO-based sensors, the annealing temperature was maintained at 600 °C and the annealing time varied; CTO-1 is the sample annealed for 6 h, while CTO-2 is the sample annealed for 30 h.

2.2. Characterization of the Samples

X-ray diffraction (XRD) patterns were analyzed using a Bruker, LinxEye D8 X-ray diffractometer in reflection mode, using Cu K α radiation (λ = 1.5406 Å) and operated at 50.0 kV and 1.0 mA. Scans were performed using a detection angle ranging from 20.0° to 70.0°. Raman spectroscopy analysis was carried out using a Renishaw 1000 spectrometer equipped with a 532 nm laser. The Raman system was calibrated using a silicon reference. All films were placed in the spectrometer using an X-Y stage and analyzed in the ranges of 200 to 800 cm⁻¹, with a laser power of 10%, an exposure time of 45 s, and an accumulation of three times per sample. Scanning electron microscopy (SEM) was conducted using a Jeol 6310F microscope. All sample images were collected using a secondary electron detector. The samples were coated with a thin layer of sputtered gold and connected to the metal stage with copper tape. Energy dispersive analysis of the X-rays was conducted using the same instrument to determine the sample composition (for the samples coated with carbon, not gold). X-ray photoelectron spectroscopy (XPS) measurements were performed using a Thermo K α spectrometer with monochromatic Al K α radiation, a dual-beam charge

Chemosensors **2024**, 12, 218 4 of 12

compensation system, and a constant pass energy of 50 eV. The binding energies were calibrated with respect to the C 1s peak at 284.6 eV.

2.3. Sensor Fabrication and Gas-Sensing Measurements

A photograph of the MEMS platform is shown in Figure 2a. Once the AACVDdeposited substrates were made, platinum wires were used to connect the alumina substrates to a pin stage, as shown in Figure 2b. Four platinum wires were used for the electrical connections; two were welded to the gold sensor trackpads on the top side of the sensor platform, and the other two were connected to the platinum heater trackpads on the bottom side. Gas-sensing measurements of the as-prepared Cr₂O₃ and CTO sensors were tested at Alphasense Ltd., UK. The working temperature and resistance of the sensors were measured and controlled by a Sensor Management System (SMS), which is designed to work with up to eight metal oxide gas sensors. It has circuits to accurately control the sensor heater temperature based on a constant-resistance setup with a digital control. The variance in the concentration of the tested gas was obtained by altering the flow rate of each gas using a mass flow controller (MFC, UFC 1100, Brooks), which was controlled by a computer program written in LabVIEW (National Instrument 2016). In a typical test cycle, the enclosed system containing the sensors was first purged with 50% humid air for 30 min; afterwards, a flow of concentrated gas analyte was passed through for 30 min, and then a flow of just humid air passed for 30 min again to clean the analyte.

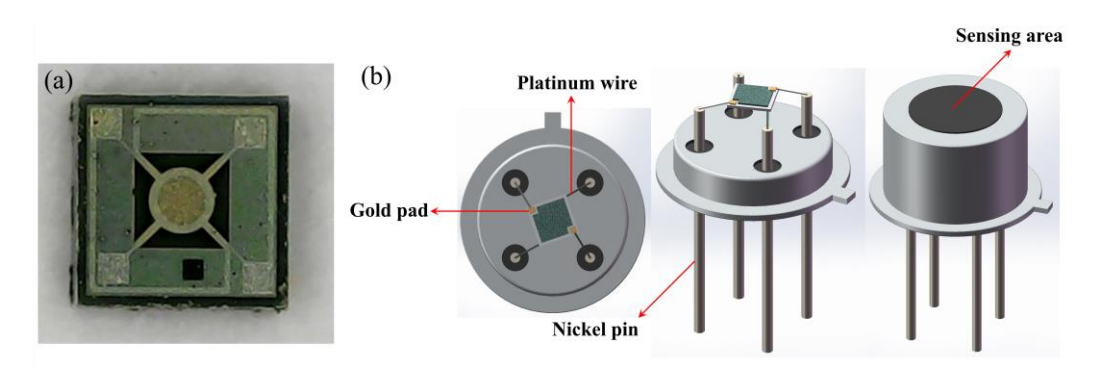


Figure 2. (a) Photograph of sensor platform, and (b) schematic diagram of a sensor connected to nickel pins via platinum wires.

3. Results and Discussion

3.1. Material Characterization

EDX analysis gave the composition of the samples as Cr1.95Ti0.05 (97.5% Cr, 2.5% Ti on a metals basis), indicating decreased incorporation of Ti into the film relative to the concentration in the precursor solution; this is commonly observed in multicomponent films deposited by AACVD and occurs due to differences in the thermal decomposition behaviour of the individual precursors. The XRD patterns of Cr₂O₃ and CTO-based sensors are shown in Figure 3, as shown in Figure 3a, the characteristic peaks at $2\theta = 24.5^{\circ}$, 33.6° , 36.2°, 41.2°, 50.2°, 54.9°, and 57.1° can be assigned to the (012), (104), (110), (113), (024), (116), and (211) planes of hexagonal phase eskolaite (JCPDS # 38-1479) [24]. The XRD patterns of corundum indicate that all of the diffraction peaks match well with the hexagonal phase Al₂O₃ (JCPDS # 46-1212), which is expected as the substrates that are made from alumina. Notably, the sharp diffraction peaks of gold (JCPDS # 04-0784) were also detected that come from the ink used for the sensing electrodes. No obvious 2θ peak shift was observed when Cr₂O₃ thin films were annealed at different temperatures (500, 600, and 700 °C) on the surface of alumina sensing platform. Figure 3b exhibits the XRD patterns of CTO thin films and the results indexed to the crystal structure of eskolaite (Cr₂O₃), corundum (Al₂O₃), and gold. The CTO patterns are in close alignment with the deposited Cr₂O₃ thin films and the result shows that no measurable change in the crystal structure is observed and peaks of TiO₂ are not present, which indicates that the full incorporation of Ti dopant

Chemosensors **2024**, 12, 218 5 of 12

into the lattice of Cr_2O_3 and no phase separation occurred within the limit of detection of XRD. Furthermore, no other impurity peaks were detected in all of the XRD patterns, demonstrating the high purity of the samples.

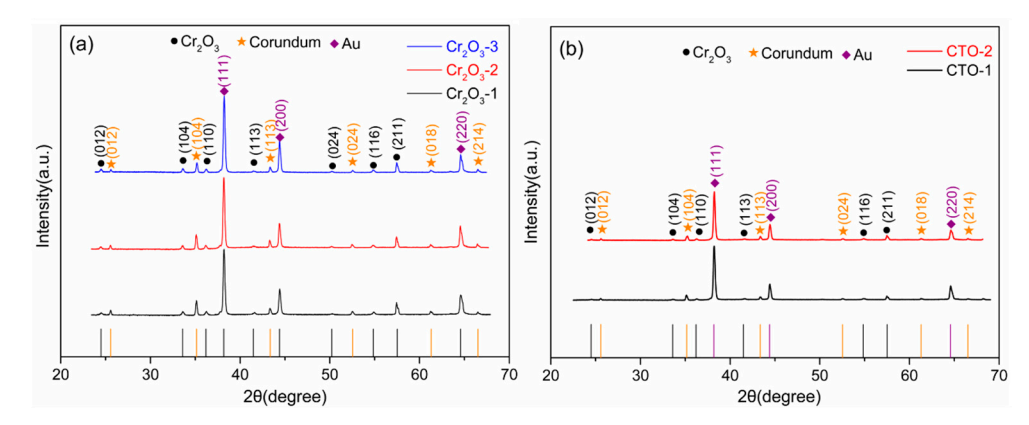


Figure 3. XRD patterns of (a) Cr_2O_3 thin film-based sensors exposed to different annealing temperatures and (b) CTO thin film-based sensors subjected to different annealing times.

The average crystal sizes of the Cr_2O_3 and CTO thin films were calculated using Scherrer's formula:

$$D = k\lambda/\beta\cos\theta. \tag{1}$$

Herein, D is the average crystal size, and all angles are in radians. For spherical crystallites, in most cases k is a constant of about 0.9. λ represents the X-ray wavelength (1.5406Å), and β is the full width at half maximum (FWHM) of the peaks of the Cr_2O_3 and CTO thin films. For the Cr_2O_3 thin films, the calculated values of the crystallite sizes are 26, 31, and 30 nm, corresponding to the different annealing temperatures of 500, 600, and 700 °C. From the results, it can be seen that the crystallite sizes may become a little bigger with the increase in annealing temperatures, but the difference is likely to be insignificant within the precision of the Scherrer estimate. In the CTO thin films, the crystallite sizes of CTO-1 and CTO-2 are 25 and 36 nm, respectively, demonstrating that the incorporation of Ti into Cr_2O_3 crystal causes no obvious influence on its crystallite size (CTO-1), but extending the annealing time from 6 h to 30 h appears to contribute to a growth in crystallite size (CTO-2). Table 1 summarizes the preparation conditions and Scherrer sizes of the different sensors.

Table 1. Preparation conditions and Scherrer sizes of the different sensors.

Samples	Annealing Temperatures (°C)	Annealing Times (h)	Scherrer Size (nm)
Cr ₂ O ₃ -1	500	24	26
Cr_2O_3-2	600	24	31
Cr_2O_3-3	700	24	30
CTO-1	600	6	25
CTO-2	600	30	36

The crystal structures were also investigated using Raman spectroscopy. Figure 4 displays the Raman spectra of the Cr_2O_3 and CTO thin films. In Cr_2O_3 , there are a total of four Raman modes observed (three E_g modes and one A_{1g} mode). Pristine Cr_2O_3 thin films exhibited three E_g vibration modes at 303, 351, and 612 cm $^{-1}$ and one intense A_{1g} mode at 553 cm $^{-1}$. The absence of characteristic TiO_2 Raman peaks for the CTO sample correlates well with the results from XRD characterization—namely, there was no phase separation on the film. The broad peak located at 721 cm $^{-1}$ has been seen previously and has been ascribed to the existence of local vibration [25].

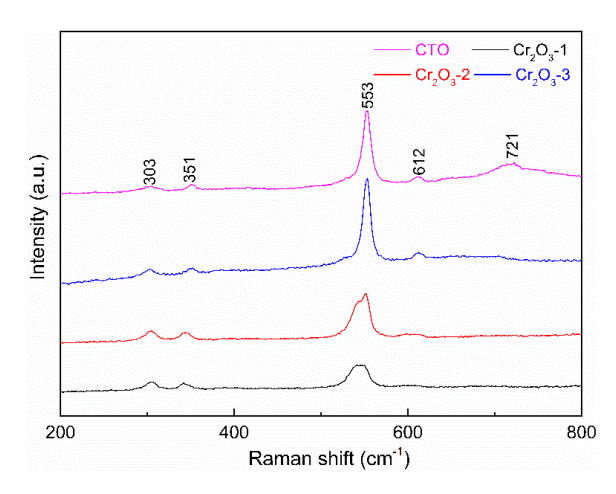


Figure 4. Raman spectra of the Cr₂O₃ and CTO thin films.

The morphologies of the as-prepared CTO thin films were characterized using SEM. As seen from the high-resolution picture (Figure 5a), the CTO thin films consisted of many uniform and well-dispersed sub-micron particles, which are spherical-like, with a diameter of 300–500 nm. It can be speculated that the particles observed in SEM are agglomerates of many smaller crystallites, due to the disparity between the particle size (SEM) and the crystallite size (Scherrer). As shown in the low-magnification SEM image (Figure 5b), the CTO particles are self-assembled to form a lamellar structure. SEM images of the $Cr_{1.95}T_{0.05}O_3$ films previously deposited (at higher temperatures) by APCVD exhibited dense and spheroidal platelets sized 1–4 μ m [14], whilst the $Cr_{1.8}Ti_{0.2}O_3$ films deposited by the ESAVD technique had a more ordered porous structure, due to the introduction of polymeric additives [15].

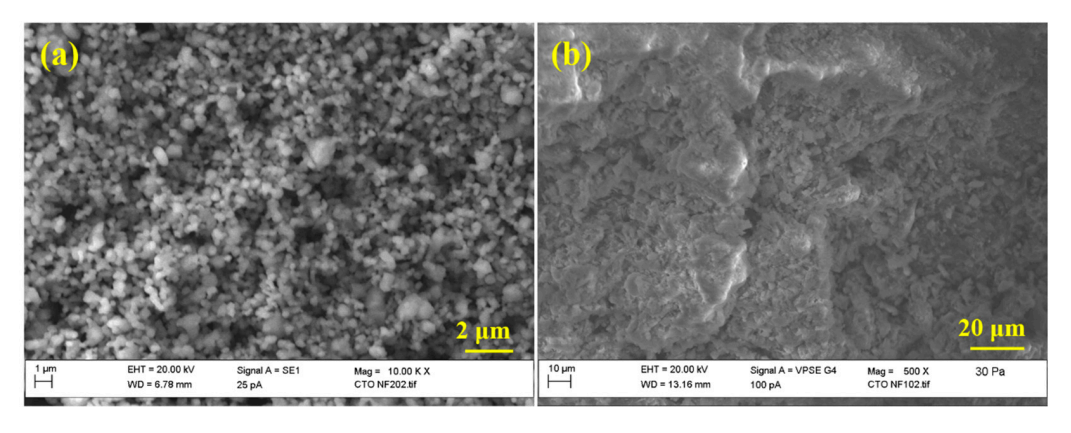


Figure 5. (a) High-resolution and (b) low-resolution SEM images of the CTO thin film.

The surface chemical composition of the as-synthesized CTO was analyzed by XPS and the results are shown in Figure 6. The XPS surface analysis was conducted using C 1s as calibration at 284.6 eV. It can be observed that the sharp peaks in the survey spectrum (Figure 6a) can be attributed to the elements of C, Ti, O, and Cr, demonstrating the successful doping of Ti into the Cr_2O_3 thin film. The high-resolution spectrum of Ti^{4+} 2p (shown in Figure 6b) is split into two peaks—of Ti^{4+} 2p_{1/2} and Ti^{4+} 2p_{3/2}—centered at 464.5 and 458.6 eV. This is in contradiction with the work of Conde-Gallardo et al. [17], who found that their $Cr_{2-x}Ti_xO_3$ films deposited by AACVD featured Ti^{3+} —although substitution by Ti^{4+} would be consistent with the decrease in conductivity they observed with increasing Ti incorporation, due to electronic compensation through the formation of electrons (which are expected to recombine with the native p-type carriers in Cr_2O_3). The Cr 2p spectrum of CTO in Figure 6c could be divided into two peaks of Cr^{3+} 2p_{1/2} and Cr^{3+} 2p_{3/2}, located at 586.6 and 576.7 eV, respectively. Figure 6d shows that the XPS spectrum of O 1s is

deconvoluted into three peaks, corresponding to Ti–O–Ti (534.2 eV), surface oxygen species (-CO_x, -OH) (532.3 eV), and Cr–O–Cr (530.4 eV), respectively [26].

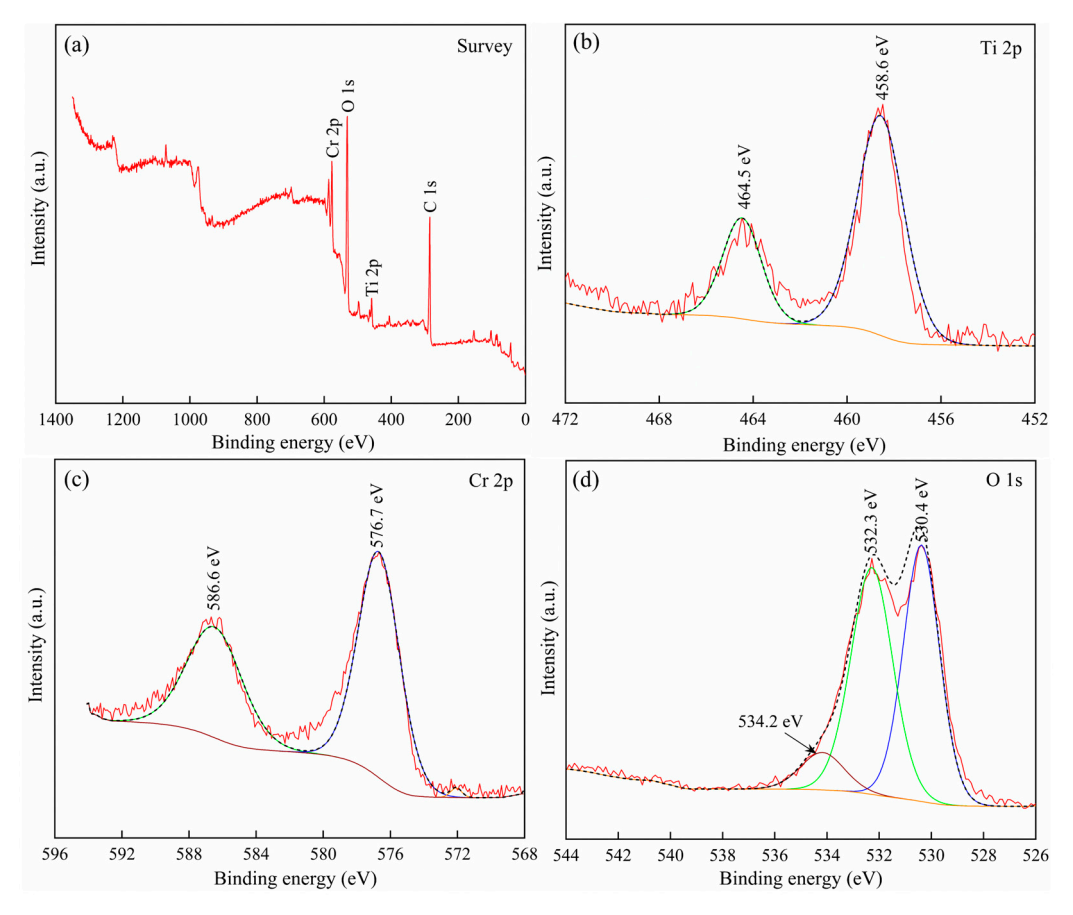


Figure 6. XPS spectra of the CTO film: (a) survey scan, (b) Ti 2p, (c) Cr 2p, and (d) O 1s.

3.2. Gas Response

Figure 7a,b show the dynamic responses of the Cr_2O_3 and CTO sensors towards C_4H_8 gas, respectively. The test conditions were set at two different concentrations of C_4H_8 gas at a relative humidity of 50% and operating temperatures of 400 and 450 °C. Each temperature was tested with three pulses of C_4H_8 gas (20-5-20 ppm). Figure 8a,b show the sensors response (resistance in gas over resistance in air, Rg/Ra) towards the different concentrations of C_4H_8 at different temperatures. The dynamic response results (Figure 7) show that the response values remained stable after the continuous test with different gas concentrations at different working temperatures. Each pulse towards the analyte was 30 min, then followed by 30 min of humid air. It can be observed that resistance values are higher for CTO as compared to resistance values of Cr_2O_3 , as expected for substitution of Cr^{3+} with Ti^{4+} , again suggesting that Ti was fully incorporated into the host lattice rather than as a separate phase. The CTO sensors also exhibited a typical p-type response upon exposure to C_4H_8 gas. All the CTO sensors prepared by AACVD show a higher response than that of the Cr_2O_3 sensors (Figure 8), although the CTO-1 sensor annealed for 6 h displayed a lower response compared to the one annealed for 30 h (CTO-2).

All the sensors were then exposed to NH_3 , at the same relative humidity and operating temperature as the C_4H_8 gas but using different concentrations (75-25-75 ppm), and the results are shown in Figure 9. Obviously, the resistance values of the sensors also all increase upon exposure to NH_3 , again showing the typical p-type property associated with Cr_2O_3/CTO . As previously, the Cr_2O_3 -2 film annealed at 600 °C shows the largest response of the three Cr_2O_3 -based sensors (Figure 8a). After doping Ti into the Cr_2O_3 thin films, the as-prepared CTO sensors exhibited a higher response to NH_3 compared to the

 Cr_2O_3 -based sensors (Figure 8b). The highest response for Cr_2O_3 at 400 °C and 75 ppm NH₃ is about 1.09, whereas the response for CTO under the same conditions is about 1.45. It is noteworthy that the annealing time influences the response of the CTO sensors to C_4H_8 and NH₃ gases.

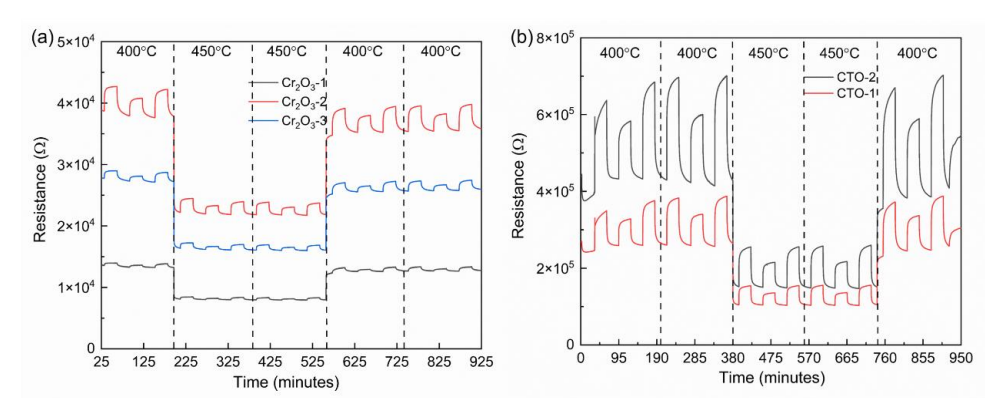


Figure 7. Change in resistance of the (a) Cr_2O_3 -based sensors and (b) CTO-based sensors to C_4H_8 gas.

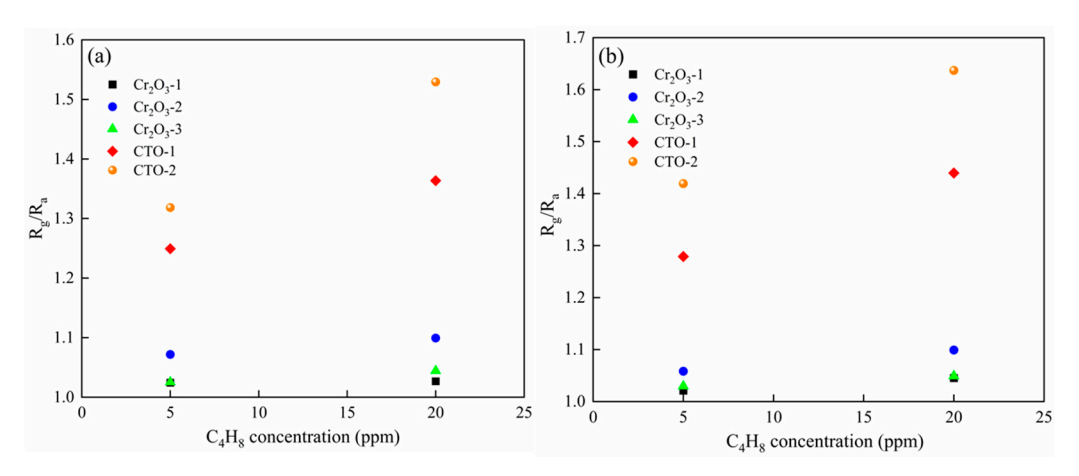


Figure 8. R_g/R_a against C_4H_8 concentration for each Cr_2O_3 and CTO sensor at different temperatures: (a) 400 °C; (b) 450 °C.

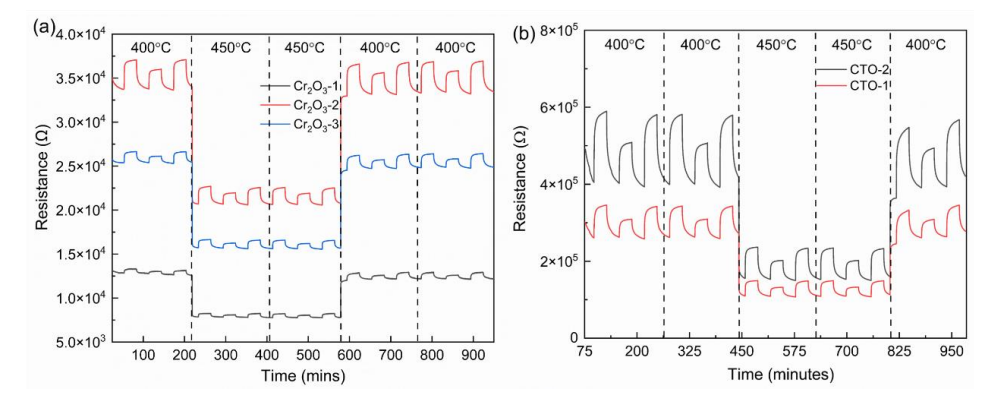


Figure 9. Change in resistance of the (a) Cr₂O₃-based sensors and (b) CTO-based sensors to NH₃.

3.3. Sensing Mechanism

In general, electron depletion theory is the most widely accepted sensing mechanism for the majority of MOSs [27]. However, an alternative self-consistent description of electronic change mediated by oxygen vacancies, rather than ionosorbed oxygen species, has been postulated for n-type MOS [28–30]. A similar mechanism for p-type materials is currently missing, despite the commonly employed electron depletion ex-planations

for p-type materials requiring the surface oxygen acceptor species to be at vastly different energy to those expected in n-type materials, which must be close to the conduction band maximum in order for their adsorption and desorption to be thermodynamically accessible, for the descriptions to work (in fact below the valence band maximum), despite there being no rationalization for such a difference to exist. However, in direct contrast to n-type materials, oxygen vacancies found in p-type ma-terials are typically 'deep' in the bandgap (further from the conduction band edge than in n-type). Consequently, they will not be ionized at normal sensor operating temper-atures (Equation (2), the electrons arising from formation of the oxygen vacancy are not ionized to free electrons but rather are 'trapped' at the vacancy). Due to the pres-ence of the (relatively) numerous (majority carrier) holes in p-type materials it is ex-pected to be thermodynamically favorable for the electrons trapped at oxygen vacan-cies (within the bandgap) to recombine with holes (in the valence band). This means formation of oxygen vacancies would reduce the concentration of primary carriers in a p-type material (Equation (3)), hence leading to a decrease in conductivity (increase in resistance) with increasing oxygen vacancy concentration (a similar explanation ex-plains the observed increase in Cr₂O₃ sensor resistance with Ti(IV)-doping (CTO); to maintain electroneutrality for every two Ti(IV) substituted onto a Cr(III) site an oxygen vacancy must be formed).

$$2O_{\mathcal{O}} \rightarrow O_2 + 2V_{\mathcal{O}}^{"} \tag{2}$$

$$2V_{\mathcal{O}}'' + 4\mathbf{h}^{\cdot} \to 2V_{\mathcal{O}}^{x}. \tag{3}$$

Therefore, under exposure to reducing conditions, the hole concentration is expected to decrease [31] and hence the resistance is expected to increase, at least at the surface of the material. As shown in Figure 10, exposure of Cr_2O_3 or CTO to NH_3 or C_4H_8 would cause the surface lattice oxygen concentration (O_O) to decrease as the lattice oxygen is consumed by oxidizing the gas species (R), i.e., the oxidation of the analyte gas causes the oxygen vacancy concentration in the sensing material to increase (V_O) , which annihilates holes (4) and causes the resistance to rise, as observed in our tests.

$$2O_O + 4h^{\cdot} + 2R \rightarrow 2RO + 2V_O^{x} \tag{4}$$

Exposure to pure air would allow the surface to re-oxidize, reducing the concentration of oxygen vacancies and hence decreasing the (surface) resistance.

Assuming that the increases in resistance observed upon introduction of the analyte gas are due to their reaction with lattice oxygen, rather than some form of direct donor (analyte)/acceptor (sensor) behavior—which seems reasonable given that the strength of any donor interaction at the elevated temperatures used here (400–450 °C) must be questionable—the relative sensitivity towards these different reducing gases would then relate either to the different thermodynamics (for a steady-state 'saturated' response) or kinetics (for a transient response) for the oxidation of the gas species by lattice oxygen, i.e., the reactivity of a given analyte species towards oxidation. Whilst we do not have a direct comparison available in our test data, a comparison of the change in resistance of our CTO sensors towards 20 ppm C_4H_8 and 25 ppm NH_3 at 450 °C (closest to steady-state response) suggests that it is thermodynamically more favorable for C_4H_8 to be oxidized by CTO (either due to the ease of oxidation or due to a more complete oxidation) at an elevated temperature (higher resistance change observed for C_4H_8 at a similar concentration).

In addition, the difference in the sensing performance between Cr_2O_3 and CTO (e.g., Figure 8) may then be attributed to the difference in the relative change in oxygen vacancy concentration between the two materials (the lower initial hole concentration in CTO, displayed schematically in Figure 10, with each Ti inducing the loss of one hole, meaning a greater relative change is measured)—although without additional analysis techniques, it cannot be discounted that the presence of Ti has a direct (e.g., catalytic) effect on the reaction.

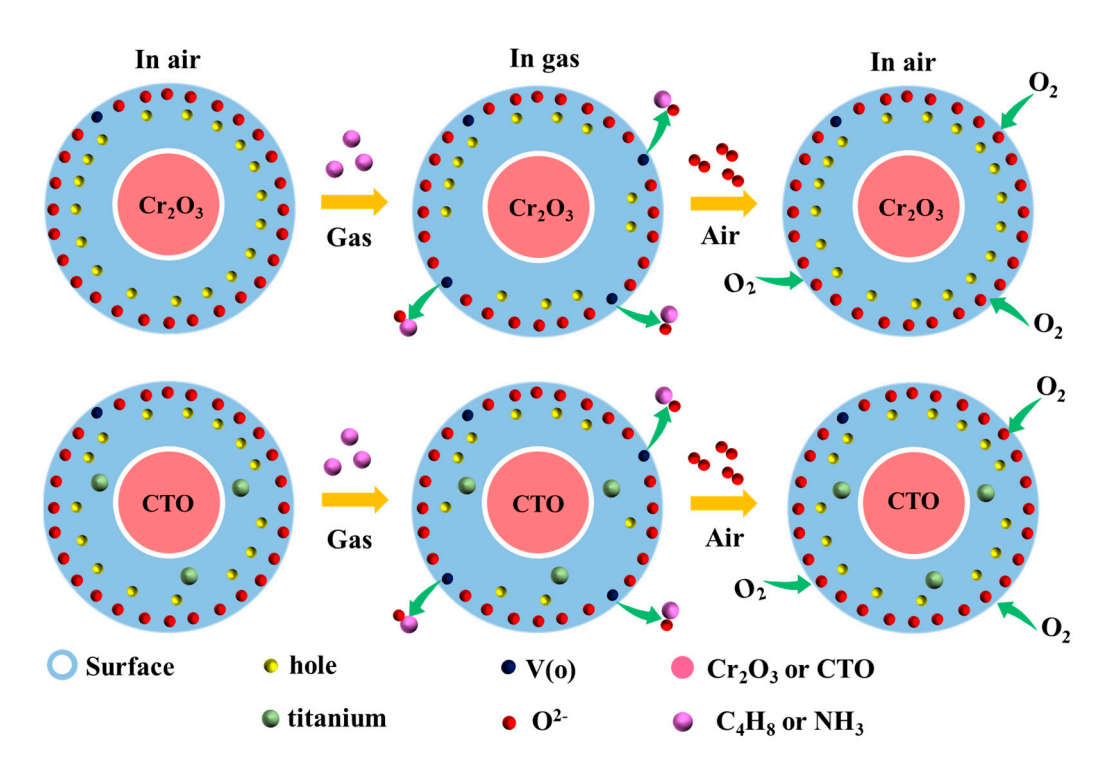


Figure 10. Schematic illustration of the possible sensing mechanism for Cr_2O_3 and CTO thin films when exposed to C_4H_8 or NH_3 .

4. Conclusions

In this work, Cr_2O_3 and CTO thin films, from $[Cr(CO)_6]$ and TBDAA precursors in a methanol solution, were deposited on the surface of an alumina platform using AACVD. Except for the patterns coming from the platform, XRD patterns for the CTO sensors only displayed the crystalline phase of eskolaite (Cr_2O_3) , which shows no indication of phase separation. XPS analysis confirmed the presence of Ti^{4+} in the CTO thin films. Doping with Ti^{4+} increased the resistance, characteristic of an n-type dopant. All the as-prepared sensors based on Cr_2O_3 and CTO thin films exhibited good sensitivity and reproducibility in response to isobutylene and ammonia gases at a humidity of 50% RH. We have postulated a new mechanism for gas sensitivity in p-type metal oxides based on a varying oxygen vacancy concentration.

Author Contributions: Conceptualization, P.Z. and J.-H.T.; methodology, C.B.; validation, J.A.C., J.S. and E.D.; formal analysis, J.L.; investigation, J.-H.T.; resources, C.B.; data curation, P.Z.; writing—original draft preparation, P.Z.; writing—review and editing, P.Z. and C.B.; visualization, Y.S.; supervision, C.B.; project administration, C.B.; funding acquisition, C.B. All authors have read and agreed to the published version of the manuscript.

Funding: This research was funded by the Engineering and Physical Sciences Research Council (grant number EP/R512400/1), the China Scholarship Council (grant number 202006080083), and the Natural Science Foundation of Hebei Province (grant number E2023202041).

Institutional Review Board Statement: Not applicable.

Informed Consent Statement: Not applicable.

Data Availability Statement: The data presented in this study are available on request from the corresponding author.

Acknowledgments: The authors thank the Engineering and Physical Sciences Research Council (EP/R512400/1), the China Scholarship Council (CSC, No. 202006080083), and the Natural Science Foundation of Hebei Province (No. E2023202041) for providing financial support. The authors would also like to thank Alphasense Ltd. for packaging the sensors.

Conflicts of Interest: Author John Saffell employed by the company Nosmotech Ltd.; Author Ehsan Danesh employed by the company Advanced Sensing Technologies Ltd. The remaining authors declare that the research was conducted in the absence of any commercial or financial relationships that could be construed as a potential conflict of interest.

References

- 1. Ayyala, S.K.; Covington, J.A. Nickel-Oxide Based Thick-Film Gas Sensors for Volatile Organic Compound Detection. *Chemosensors* **2021**, *9*, 247. [CrossRef]
- 2. Agbroko, S.O.; Covington, J. A novel, low-cost, portable PID sensor for the detection of volatile organic compounds. *Sens. Actuators B* **2018**, 275, 10–15. [CrossRef]
- 3. Ding, C.; Ma, Y.; Lai, X.; Yang, Q.; Xue, P.; Hu, F.; Geng, W. Ordered Large-Pore Mesoporous Cr₂O₃ with Ultrathin Framework for Formaldehyde Sensing. ACS Appl. *Mater. Interfaces* **2017**, *9*, 18170–18177. [CrossRef] [PubMed]
- 4. Jin, H.; Huang, Y.; Jian, J. Plate-like Cr₂O₃ for highly selective sensing of nitric oxide. *Sens. Actuators B* **2015**, 206, 107–110. [CrossRef]
- 5. Zhang, M.; Sui, N.; Wang, R.; Zhang, T. The effect of shell thickness on gas sensing properties of core-shell fibers. *Sens. Actuators B* **2021**, 332, 129456. [CrossRef]
- 6. Yamazoe, N. Toward innovations of gas sensor technology. Sens. Actuators B Chem. 2005, 108, 2–14. [CrossRef]
- 7. Moumen, A.; Kumarage, G.C.W.; Comini, E. P-Type Metal Oxide Semiconductor Thin Films: Synthesis and Chemical Sensor Applications. *Sensors* **2022**, 22, 1359. [CrossRef]
- 8. Song, B.-Y.; Liu, L.-H.; Yang, M.; Zhang, X.-F.; Deng, Z.-P.; Xu, Y.-M.; Huo, L.-H.; Gao, S. Biotemplate-directed synthesis of Cr₂O₃ mesoporous monotubes for enhanced sensing to trace H₂S gas. *Sens. Actuators B* **2022**, *369*, 132294. [CrossRef]
- Liu, B.; Han, W.; Li, X.; Li, L.; Tang, H.; Lu, C.; Li, Y.; Li, X. Quasi metal organic framework with highly concentrated Cr₂O₃ molecular clusters as the efficient catalyst for dehydrofluorination of 1,1,1,3,3-pentafluoropropane. *Appl. Catal. B* 2019, 257, 117939. [CrossRef]
- 10. Cheng, J.; Li, Y.; Zhong, J.; Lu, Z.; Wang, G.; Sun, M.; Jiang, Y.; Zou, P.; Wang, X.; Zhao, Q.; et al. Molecularly imprinted electrochemical sensor based on biomass carbon decorated with MOF-derived Cr₂O₃ and silver nanoparticles for selective and sensitive detection of nitrofurazone. *Chem. Eng. J.* **2020**, *398*, 125664. [CrossRef]
- 11. Atkinson, A.; Levy, M.R.; Roche, S.; Rudkin, R.A. Defect properties of Ti-doped Cr₂O₃. Solid State Ion. **2006**, 177, 1767–1770. [CrossRef]
- 12. Henshaw, G.S.; Dawson, D.H.; Williams, D.E. Selectivity and composition dependence of response of gas-sensitive resistors. Part 2.—Hydrogen sulfide response of Cr_{2-x}Ti_xO_{3+y}. *J. Mater. Chem.* **1995**, *5*, 1791–1800. [CrossRef]
- 13. Blacklocks, A.N.; Atkinson, A.; Packer, R.J.; Savin, S.L.P.; Chadwick, A.V. An XAS study of the defect structure of Ti-doped α-Cr₂O₃. *Solid State Ion.* **2006**, 177, 2939–2944. [CrossRef]
- 14. Shaw, G.A.; Pratt, K.F.E.; Parkin, I.P.; Williams, D.E. Gas sensing properties of thin film (≤3 μm) Cr_{2−x}Ti_xO₃ (CTO) prepared by atmospheric pressure chemical vapour deposition (APCVD), compared with that prepared by thick film screen-printing. *Sens. Actuators B* **2005**, *104*, 151–162. [CrossRef]
- 15. Du, J.; Wu, Y.; Choy, K.-L. Controlled synthesis of gas sensing Cr_{2-x}Ti_xO₃ films by electrostatic spray assisted vapour deposition and their structural characterisation. *Thin Solid Films* **2006**, 497, 42–47. [CrossRef]
- 16. Du, J.; Wu, Y.; Choy, K.-L.; Shipway, P.H. Structure, properties and gas sensing behavior of Cr_{2-x}Ti_xO₃ films fabricated by electrostatic spray assisted vapour deposition. *Thin Solid Films* **2010**, *519*, 1293–1299. [CrossRef]
- 17. Conde-Gallardo, A.; Cruz-Orea, A.; Zelaya-Angel, O.; Bartolo-Pèrez, P. Electrical and optical properties of Cr_{2-x}Ti_xO₃ thin films. *J. Phys. D Appl. Phys.* **2008**, *41*, 205407. [CrossRef]
- 18. Vallejos, S.; Di Maggio, F.; Shujah, T.; Blackman, C. Chemical Vapour Deposition of Gas Sensitive Metal Oxides. *Chemosensors* **2016**, *4*, 4. [CrossRef]
- 19. Ehsan, M.A.; Shah, S.S.; Basha, S.I.; Hakeem, A.S.; Aziz, M.A. Recent Advances in Processing and Applications of Heterobimetallic Oxide Thin Films by Aerosol-Assisted Chemical Vapor Deposition. *Chem. Rec.* **2022**, 22, e202100278. [CrossRef]
- 20. Srirattanapibul, S.; Nakarungsee, P.; Issro, C.; Tang, I.M.; Thongmee, S. Enhanced room temperature NH₃ sensing of rGO/Co₃O₄ nanocomposites. *Mater. Chem. Phys.* **2021**, 272, 125033. [CrossRef]
- 21. Dey, A. Semiconductor metal oxide gas sensors: A review. Mater. Sci. Eng. B 2018, 229, 206–217. [CrossRef]
- 22. Natarajamani, G.S.; Kannan, V.P.; Madanagurusamy, S. Synergistically enhanced NH₃ gas sensing of graphene oxide-decorated Nano-ZnO thin films. *Mater. Chem. Phys.* **2024**, *316*, 129036. [CrossRef]
- 23. Li, D.; Han, D.; Chen, Y.; Hong, Y.; Duan, Q.; Wang, H.; He, X.; Zhao, L.; Wang, W.; Sang, S. GaN/rGO nanocomposite gas sensor for enhanced NH₃ sensing performances at room temperature. *Sens. Actuators B* **2024**, 403, 135209. [CrossRef]
- 24. Song, B.-Y.; Zhang, X.-F.; Huang, J.; Cheng, X.-L.; Deng, Z.-P.; Xu, Y.-M.; Huo, L.-H.; Gao, S. Porous Cr₂O₃ Architecture Assembled by Nano-Sized Cylinders/Ellipsoids for Enhanced Sensing to Trace H₂S Gas. *ACS Appl. Mater. Interfaces* **2022**, *14*, 22302–22312. [CrossRef]
- 25. Dutta, S.; Pandey, A.; Leeladhar; Jain, K.K. Growth and characterization of ultrathin TiO₂-Cr₂O₃ nanocomposite films. *J. Alloys Compd.* **2017**, 696, 376–381. [CrossRef]

26. Baraskar, P.; Chouhan, R.; Agrawal, A.; Choudhary, R.J.; Sen, P. Weak ferromagnetism at room temperature in Ti incorporated Cr₂O₃ thin film. *Phys. B* **2019**, *571*, 36–40. [CrossRef]

- 27. Williams, D.E. Semiconducting oxides as gas-sensitive resistors. Sens. Actuators B Chem. 1999, 57, 1–16. [CrossRef]
- 28. Blackman, C. Do We Need "Ionosorbed" Oxygen Species? (Or, "A Surface Conductivity Model of Gas Sensitivity in Metal Oxides Based on Variable Surface Oxygen Vacancy Concentration"). ACS Sens. 2021, 6, 3509–3516. [CrossRef]
- 29. Kucharski, S.; Ferrer, P.; Venturini, F.; Held, G.; Walton, A.S.; Byrne, C.; Covington, J.A.; Ayyala, S.K.; Beale, A.M.; Blackman, C. Direct in situ spectroscopic evidence of the crucial role played by surface oxygen vacancies in the O₂-sensing mechanism of SnO₂. *Chem. Sci.* **2022**, *13*, 6089–6097. [CrossRef]
- 30. Cox, D.F.; Fryberger, T.B.; Semancik, S. Oxygen vacancies and defect electronic states on the SnO₂ (110)-1 × 1 surface. *Phys. Rev. B* **1988**, 38, 2072–2083. [CrossRef]
- 31. Gunkel, F.; Christensen, D.V.; Chen, Y.Z.; Pryds, N. Oxygen vacancies: The (in)visible friend of oxide electronics. *Appl. Phys. Lett.* **2020**, *116*, 120505. [CrossRef]

Disclaimer/Publisher's Note: The statements, opinions and data contained in all publications are solely those of the individual author(s) and contributor(s) and not of MDPI and/or the editor(s). MDPI and/or the editor(s) disclaim responsibility for any injury to people or property resulting from any ideas, methods, instructions or products referred to in the content.